SCIENCE CHINA PRESS

SCIENCE CHINA Life Sciences
life.scichina.com link.springer.com
https://doi.org/10.1007/s11427-023-2364-3

RESEARCH PAPER

The role of corneal endothelium in macular corneal dystrophy development and recurrence

Bi-Ning Zhang[1,2,3], Benxiang Qi[1,2,3], Chunxiao Dong[1,3,4], Bin Zhang[1,2,3], Jun Cheng[1,2,3], Xin Wang[2,3,5], Suxia Li[2,3,5], Xiaoyun Zhuang[1,3,6], Shijiu Chen[1,3,4], Haoyun Duan[1,2,3], Dewei Li[1,2,3], Sujie Zhu[7], Guoyun Li[8,9], Yihai Cao[10], Qingjun Zhou[1,2,3*] & Lixin Xie[1,2,3*]

[1]Eye Institute of Shandong First Medical University, Qingdao Eye Hospital of Shandong First Medical University, Qingdao 266071, China;
[2]State Key Laboratory Cultivation Base, Shandong Provincial Key Laboratory of Ophthalmology, Qingdao 266071, China;
[3]School of Ophthalmology, Shandong First Medical University, Qingdao 250021, China;
[4]Department of Medicine, Qingdao University, Qingdao 266071, China;
[5]Eye Institute of Shandong First Medical University, Eye Hospital of Shandong First Medical University (Shandong Eye Hospital), Jinan 250021, China;
[6]Department of Ophthalmology, School of Clinical Medicine, Weifang Medical University, Weifang 261072, China;
[7]Institute of Translational Medicine, College of Medicine, Qingdao University, Qingdao 266071, China;
[8]Key Laboratory of Marine Drugs of Ministry of Education, Shandong Provincial Key Laboratory of Glycoscience and Glycotechnology, School of Medicine and Pharmacy, Ocean University of China, Qingdao 266071, China;
[9]Laboratory for Marine Drugs and Bioproducts, Pilot National Laboratory for Marine Science and Technology (Qingdao), Qingdao 266071, China;
[10]Department of Microbiology, Tumor and Cell Biology, Biomedicum, Karolinska Institutet, Stockholm 17177, Sweden

*Corresponding authors (Qingjun Zhou, email: qjzhou2000@hotmail.com; Lixin Xie, email: lixin_xie@hotmail.com)

Received 9 February 2023; Accepted 10 May 2023; Published online 17 July 2023

Macular corneal dystrophy (MCD) is a progressive, bilateral stromal dystrophic disease that arises from mutations in carbohydrate sulfotransferase 6 (*CHST6*). Corneal transplantation is the ultimate therapeutic solution for MCD patients. Unfortunately, postoperative recurrence remains a significant challenge. We conducted a retrospective review of a clinical cohort comprising 102 MCD patients with 124 eyes that underwent either penetrating keratoplasty (PKP) or deep anterior lamellar keratoplasty (DALK). Our results revealed that the recurrence rate was nearly three times higher in the DALK group (39.13%, 9/23 eyes) compared with the PKP group (10.89%, 11/101 eyes), suggesting that surgical replacement of the corneal endothelium for treating MCD is advisable to prevent postoperative recurrence. Our experimental data confirmed the robust mRNA and protein expression of CHST6 in human corneal endothelium and the rodent homolog CHST5 in mouse endothelium. Selective knockdown of wild-type *Chst5* in mouse corneal endothelium ($AC^{siChst5}$), but not in the corneal stroma, induced experimental MCD with similar extracellular matrix synthesis impairments and corneal thinning as observed in MCD patients. Mice carrying *Chst5* point mutation also recapitulated clinical phenotypes of MCD, along with corneal endothelial abnormalities. Intracameral injection of wild-type *Chst5* rescued the corneal impairments in $AC^{siChst5}$ mice and retarded the disease progression in *Chst5* mutant mice. Overall, our study provides new mechanistic insights and therapeutic approaches for MCD treatment by highlighting the role of corneal endothelium in MCD development.

macular corneal dystrophy | recurrence | corneal endothelium | keratan sulfate | penetrating keratoplasty

INTRODUCTION

Macular corneal dystrophy (MCD) is an autosomal recessive inherited disease that manifests as grey-white, irregular opacities in the corneal stroma. It is classified as a stromal dystrophy according to the International Classification of Corneal Dystrophies (IC3D) (Lisch and Weiss, 2019; Weiss et al., 2015). The disease usually progresses in both eyes, starting in the first decade of life and leading to significant vision loss (Hassell et al., 1980). Patients with MCD typically require corneal transplantation in middle age (Hassell et al., 1980). In addition to the shortage of available donor cornea tissues for transplantation (Gain et al., 2016), MCD patients also face a high risk of recurrence and may require re-grafting (Klintworth et al., 1983).

In a previous retrospective study, we followed 51 MCD patients over an 18-year period and found that patients undergoing penetrating keratoplasty (PKP) had a lower recurrence rate and delayed recurrence onset compared with those undergoing deep anterior lamellar keratoplasty (DALK) (Cheng et al., 2013). The five-year recurrence rate of PKP is 7.7% while that of DALK was 49.5% (Cheng et al., 2013). In another study that included 84 eyes with MCD and lattice corneal dystrophy (LCD), which also belongs to stromal dystrophies, MCD patients with DALK had a progressive decrease of corneal endothelial density, which was not observed in the LCD group (Kawashima et al., 2006). A more recent study involving 109 MCD eyes with PKP and 21 MCD eyes with DALK found a higher graft survival rate in the PKP group than in the DALK group (Reddy et al., 2015). These results suggest that DALK might not be the optimal surgery for MCD. We hypothesized that the corneal endothelium, which is not replaced in DALK but is replaced in PKP, may play a role in the recurrence and clinical outcomes of MCD.

The pathogenesis of MCD has been linked to mutations in *CHST6* (Akama et al., 2000; Lisch and Weiss, 2019), which codes for corneal *N*-acetylglucosaminyl-6-*O*-sulfotransferase (cGn6ST), an enzyme that transfers sulfate from 3′-phosphoadenosine 5′-phosphosulphate (PAPS) to the 6-*O* positions of the *N*-acetylglucosamine (GlcNAc) during the biosynthesis of keratin sulfate (KS) (Akama et al., 2000; Caterson and Melrose, 2018; Quantock et al., 2010). KS glycosaminoglycan (GAG) constitutes the major corneal proteoglycans including lumican, keratocan, and mimecan, which are essential in maintaining corneal transparency (Young et al., 2005). The mouse homolog of human *CHST6*, *Chst*5, is biologically equivalent in function (Akama et al., 2001).

To investigate the potential involvement of corneal endothelium in MCD, a retrospective analysis of MCD recurrence over 30 years was conducted at our hospital. The mRNA and protein expression of CHST6 in human corneas and CHST5 in mouse corneas were examined. Additionally, models with genetic downregulation of *Chst*5 in corneal stroma and endothelium were developed for the validation of endothelial involvement during MCD. A mouse model carrying a CHST5 R50H point mutation was created to assess its endothelial phenotypes. Finally, corneal endothelial overexpression was utilized to conduct rescue experiments. Our findings support the involvement of endothelial cells in MCD pathogenesis and recurrence.

RESULTS

MCD patients displayed corneal endothelial abnormities

In severe cases of MCD, two types of corneal transplantation, PKP and DALK, are commonly used. PKP involves the replacement of the full-thickness host cornea with a full-thickness donor cornea, as depicted in Figure 1A. In contrast, DALK entails manual dissection of the corneal stroma with about 100 μm transparent stroma left together with the Descemet's membrane (DM) and endothelium (Figure 1A). The visual acuity of MCD patients receiving DALK relies on the donor button and their residual corneal tissues, especially the endothelium. Endothelial black holes were already observed through corneal confocal microscopy in a six-year-old girl with early-stage MCD (Figure 1B), implying an early involvement of endothelium in MCD. In MCD patients who undergo PKP, the endothelial density (3,534 cells per mm^2) and morphology remain healthy (Figure 1C). However, a recurrent MCD patient receiving DALK exhibited abundant abnormal deposits in the endothelial layer and decreased endothelial density (1,543 cells per mm^2) (Figure 1D), indicating the crucial role of the endothelium in maintaining corneal transparency.

The recurrence of MCD is defined as the presence of MCD haze that extends into the graft button, which is observable under the slit lamp examination irrespective of changes in visual acuity. An example of a typical recurrence case after 11 years of PKP showed haze likely originating from the peripheral host cornea and spreading towards the edges of the graft, as observed through optical coherence tomography (OCT) (Figure 1E). On the other hand, a typical recurrence case after 8.7 years of DALK showed haze developing from the bottom of the host cornea (Figure 1F), indicating a possible association between the residual endothelium and MCD recurrence in DALK.

Endothelium reservation is associated with a higher MCD recurrence rate

A total of 102 MCD patients with 124 eyes who underwent corneal transplantation at Qingdao Eye Hospital were retrospectively reviewed. Among them, 10.89% (11/101) of MCD eyes receiving PKP and 39.13% (9/23) of eyes receiving DALK by manual dissection were diagnosed with recurrences (Figure 1G). The MCD recurrent rate was significantly associated with the surgical method (P=0.017, χ^2 test). The average time to recurrence was significantly longer for eyes receiving PKP, with 6.38±3.34 years compared with 2.56±2.71 years for eyes receiving DALK (P=0.017, Mann-Whitney U test). More than half of the recurrent eyes in the PKP group still had functional grafts at seven years post-surgery, whereas half of the recurrent eyes in the DALK group had graft failed within the first two years (Figure 1H). In summary, MCD patients receiving PKP had a lower recurrence rate and a longer graft survival time than those receiving DALK, suggesting a potential contribution of the host endothelium to MCD recurrence.

KS sulfation sulfotransferase enriches in corneal endothelium

MCD is a condition characterized by the accumulation of unsulfated GAGs in the cornea, leading to progressive cloudiness (Figure 2A). In addition to stromal deposits, we observed intracellular and extracellular GAG deposits in the endothelium of MCD patients (Figure 2B). The sulfation of corneal KS is catalyzed by the *CHST6*-encoded sulfotransferase. To evaluate the expression pattern of CHST6 and CHST5, we manually dissected the three corneal layers from both human and mouse corneal samples and used qPCR to verify the specificity of layer separation by detecting genes typically enriched in each layer. As expected, the epithelial marker *KRT12*, stromal marker *KERA*, and endothelial marker *ATP1A1* or *Col8a1* were enriched in their respective corneal layers (Figure S1 in Supporting Information). We found that *CHST6* mRNA is abundantly expressed in keratocytes, but comparative *CHST6* was also detected in corneal endothelium (Figure 2C). Interestingly, CHST6 protein staining was more pronounced in the endothelium than in sparsely stained keratocytes (Figure 2D; Figure S2 in Supporting Information). Likewise, CHST5 mRNA and protein levels were higher in the mouse endothelium than in other corneal layers (Figure 2E and F).

Knockdown of endothelial *Chst*5 contributes to the corneal stromal lesions

Although CHST6 and CHST5 expression was abundantly expressed in the corneal endothelium, it was unclear whether endothelial *Chst*5 deficiency could induce MCD phenotypes. To investigate this, we used adeno-associated virus serotype 9 (AAV9)-siRNA to construct a loss-of-function model, which was injected into the anterior chamber ($AC^{siChst5}$) to transfect the corneal endothelium (Figure 3A). The knockdown of endothelial *Chst*5 was approximately 45% (Figure 3B). During the intracameral injection, the needle also passed through the corneal stroma. To exclude the possibility that the corneal lesions were caused by the leakage of AAV into the stroma, we created an intrastromal control model by directly injecting the AAV9-siRNA

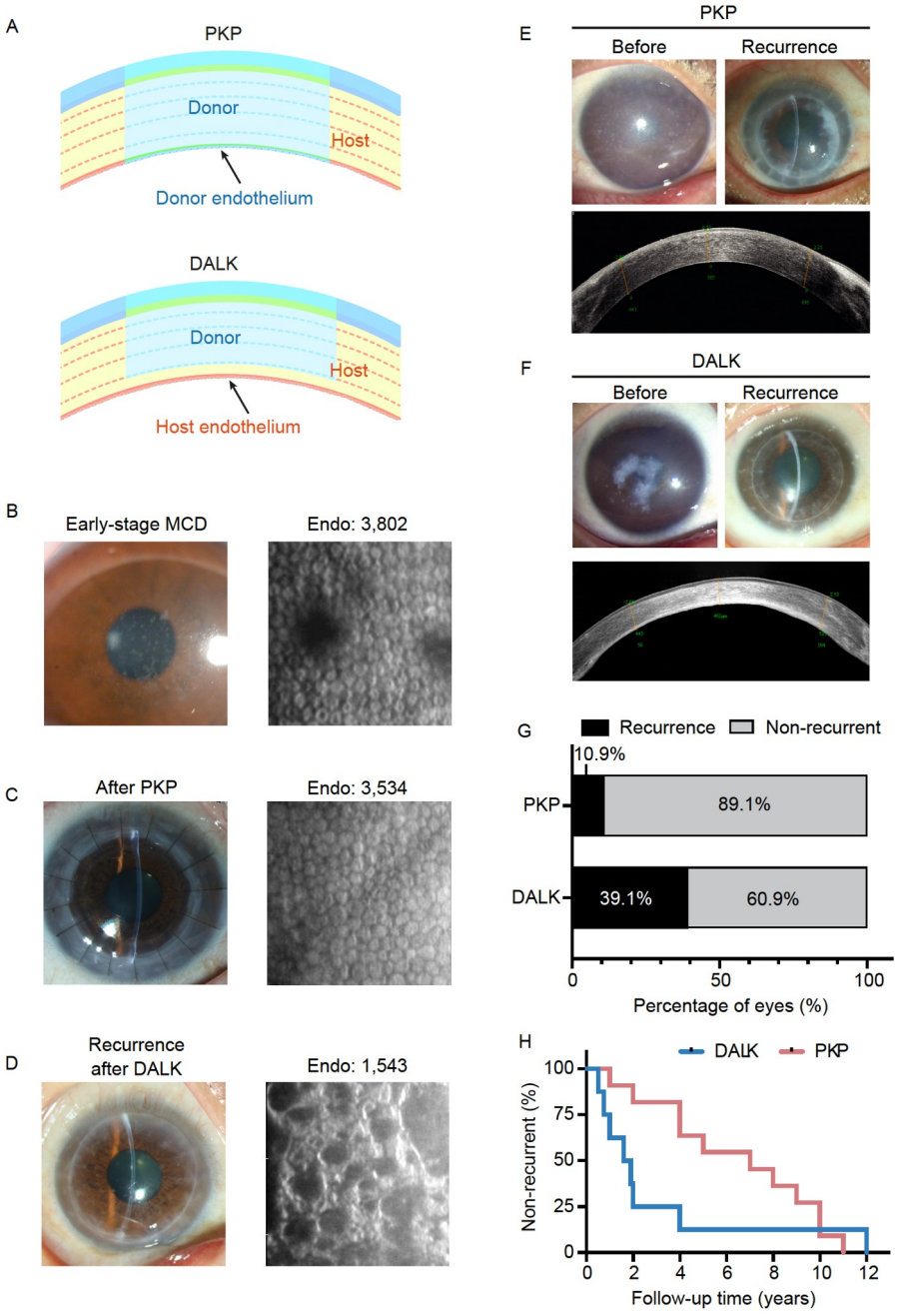

Figure 1. Recurrence and corneal endothelial phenotypes in MCD. A, Schematic diagram of corneal transplantation strategies for MCD patients in our cohort. B, Slit lamp corneal photo and endothelial confocal microscopy image of a 6-year-old girl with early-stage MCD. Corneal density is 3,802 cells per mm^2. C, Slit lamp corneal photo and endothelial confocal microscopy image of an MCD patient after PKP. D, Slit lamp corneal photo and endothelial confocal microscopy image of an MCD patient after DALK. She had MCD recurrence in her right eye. E, Slit lamp photos and OCT image of a typical recurrence case before and after PKP. F, Slit lamp photos and OCT image of a typical recurrence case before and after DALK. G, Recurrence rate of MCD eyes receiving PKP and DALK. H, Survival curve of the graft in recurrent eyes after DALK and PKP.

into the corneal stroma ($Str^{siChst5}$) (Figure 3A). In this intrastromal injection model, the stromal *Chst5* was reduced by around 61% (Figure 3B). To confirm the knockdown effect of intrastromal injection of AAV9-siRNA, we constructed a positive control targeting the stromal marker *Kera* and carrying a GFP tag. GFP was observed in the stromal layer throughout the whole cornea (Figure S3A in Supporting Information), and qPCR confirmed that the stromal *Kera* was reduced by around 91% after intrastromal injection (Figure S3B in Supporting Information). A control siRNA sequence targeting no gene was packaged to the same AAV9 vector and served as a control plasmid (siCon). Intracameral injection (AC^{siCon}) and intrastromal infection (Str^{siCon}) were performed following the same protocol.

The presence of MCD-like opacities in mice was confirmed by slit lamp and false-color OCT, with 11.3% (6/53) of the $AC^{siChst5}$ group developing such opacities, while none of the AC^{siCon} (0/32), $Str^{siChst5}$ (0/14), Str^{siCon} (0/9) mice developed them (Figure 3C and D; Figure S4A and B in Supporting Information). To access the accumulation of acid mucopolysaccharide, which is a hallmark of MCD stroma, we performed alcian

https://doi.org/10.1007/s11427-023-2364-3

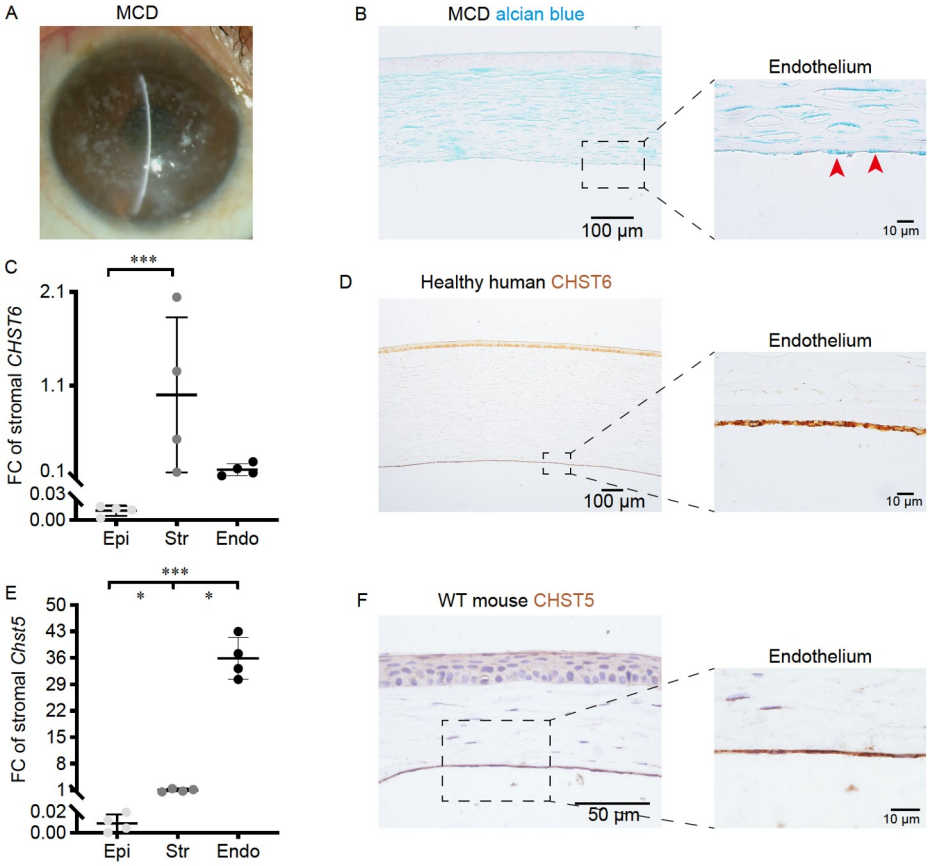

Figure 2. CHST6 is enriched in corneal endothelium. A, Eye photo of a typical MCD patient. B, Alcian blue staining of the corresponding corneal section. Arrowheads indicate positive abnormal deposits in the intracellular space of endothelial cells. n=3. C, Relative expression of *CHST6* in the epithelium and endothelium compared with stromal *CHST6*. n=4. P=0.01 between Epi and Str; P=0.718 between Str and Endo. Kruskal-Wallis Test with all pairwise multiple comparisons. D, Immunohistochemistry staining of CHST6 (brown) in healthy human cornea. E, Relative expression of *Chst5* in the epithelium and endothelium compared with stromal *Chst5*. n=4. P=0.029 between Epi and Str, Str and Endo; P=0.005 between Epi and Endo. Kruskal-Wallis Test with all pairwise multiple comparisons. F, Immunohistochemistry staining of CHST5 (brown) in a WT mouse cornea. n=3.

blue staining on randomly selected mice from each experimental group. We found 81.8% (9/11) of the $AC^{siChst5}$ mice displayed positive staining in the interfibrillar spaces, whereas none of the AC^{siCon} (0/3), $Str^{siChst5}$ (0/3), Str^{siCon} (0/3) mice stained positive (Figure 3E; Figure S4C in Supporting Information). KS is the major GAG in the cornea and proper sulfation of KS is essential for corneal transparency. We stained the sulphated KS in our *Chst5* knockdown mice with monoclonal antibody 5D4 and found that KS staining was diminished in the $AC^{siChst5}$ mice, while relatively homogenous staining was observed in the other three groups (Figure 3F; Figure S4D in Supporting Information). Finally, we observed irregularly shaped endothelial cells with discontinuous membranes in the $AC^{siChst5}$ group after staining with alizarin red S, but not in the other three groups (Figure 3G; Figure S4E in Supporting Information).

The manifestation of enlarged collagen fibers, reduced collagen interfibrillar spacing, and thinner corneal stroma are the features of MCD patients (Palka et al., 2010). To further characterize the structural changes of the fibrils, we utilized transmission electron microscopy (TEM). TEM analysis showed that the diameters of collagen fibrils were increased in the $AC^{siChst5}$ group as compared with wild-type (WT) and $Str^{siChst5}$ mice (Figure 3H). The average collagen fibril diameter was (32.22±2.13) nm in the WT, (34.47±2.28) nm in the $Str^{siChst5}$ group, and (39.23 ±3.69) nm in the $AC^{siChst5}$ group, respectively (Figure 3H). Though corneal opacification was not observed in the $Str^{siChst5}$ group, the diameter of the stromal collagen fibrils was slightly increased (Figure 3H). In summary, the knockdown of mouse endothelial *Chst5* efficiently induced experimental MCD.

Extracellular matrix profile alterations in experimental MCD corneas

In order to confirm corneal lesions in $AC^{siChst5}$ mice and gain a deeper understanding of corneal changes during MCD development, corneas were collected one month after endothelial *Chst5* knockdown for RNA sequencing (Figure 4A). A total of 561 differentially expressed genes (DEGs) were identified between $AC^{siChst5}$ and AC^{siCon}, with 380 genes upregulated (Figure S5A in Supporting Information) and 181 genes downregulated in $AC^{siChst5}$ (Figure 4B). The top upregulated genes were enriched in categories of "protein binding" and "receptor binding" (Figure S5B in Supporting Information), while the top downregulated term was "extracellular matrix structural constituent" (Figure 4C). Representative genes in the downregulated term mainly consisted of collagen genes (Figure 4D). This decline in expression was further confirmed by qPCR (Figure 4E). Since the stroma accounts for over 90% of the total corneal thickness, the reduction in the extracellular matrix after *Chst5* knockdown is believed to contribute to a thinner cornea. Indeed, the average

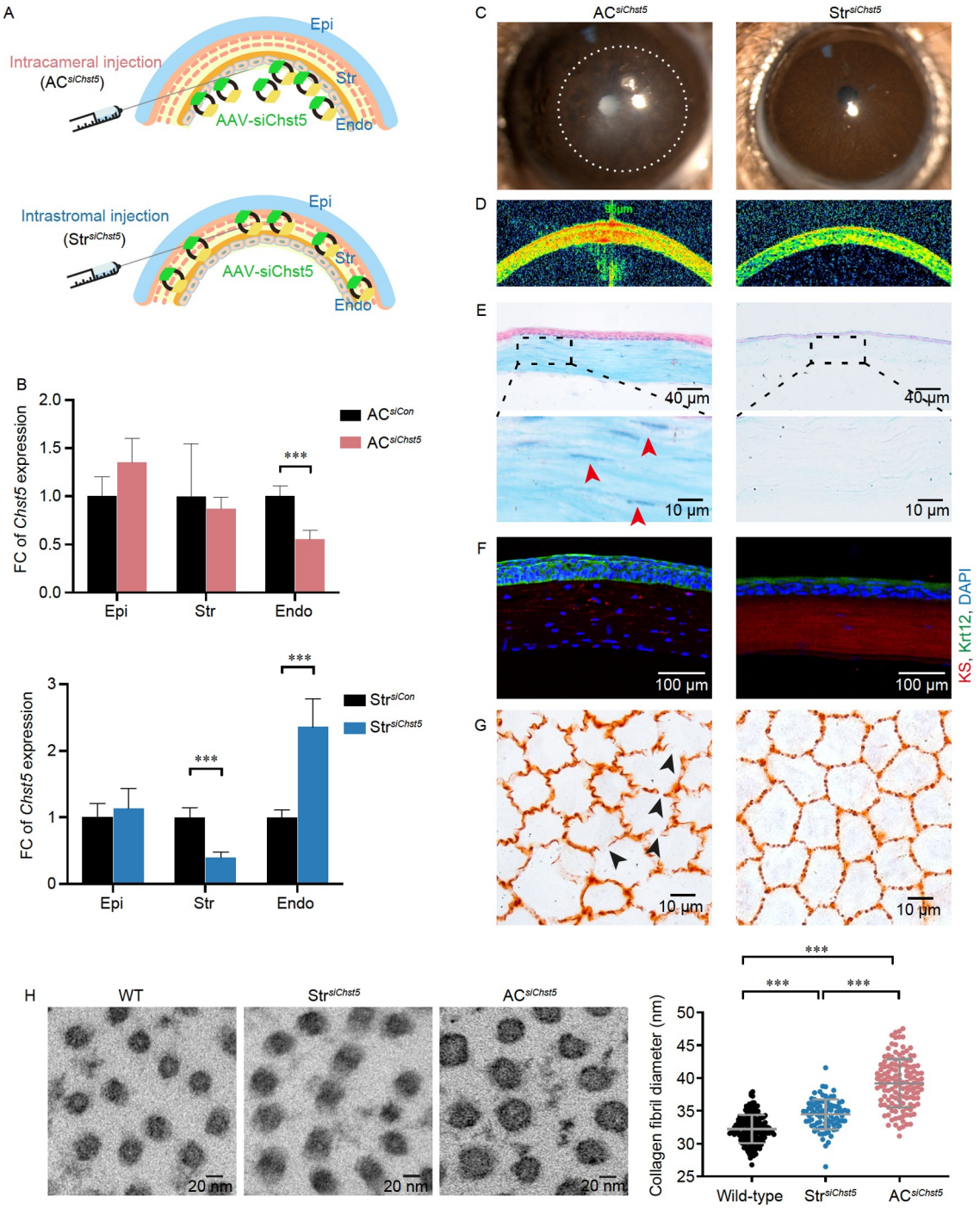

Figure 3. Endothelial *Chst5* knockdown contributes to MCD phenotype. A, Schematic diagram illustrating the intracameral injection and the intrastromal injection routes used for *Chst5* knockdown. B, Relative expression of *Chst5* in the corneal layers of mice receiving AC^{siChst5} and Str^{siChst5} injections. The AC^{siChst5} group showed a significant decrease in endothelial *Chst5* compared with the control AC^{siCon} group. n=8. P=0.002 for the endothelium. t-test. The Str^{siChst5} group showed a significant decrease in stromal *Chst5* compared with the Str^{siCon} group. n=8. P<0.001 for stroma and P=0.006 for endothelium. t-test. C and D, Slit lamp photos and OCT images of a representative mouse in each group. The AC^{siChst5} mouse developed corneal opacification (white dashed circle) while the Str^{siChst5} group did not show any obvious corneal changes. Number of mice developed opacity: AC^{siChst5} (6/53), Str^{siChst5} (0/14). E, Alcian blue staining of mouse corneas. Blue deposits were present throughout the full thickness of the AC^{siChst5} stroma, but not in the Str^{siChst5} group. Number of mice developed positive staining: AC^{siChst5} (9/11), Str^{siChst5} (0/3). F, Immunostaining of KS and Krt12 in mouse corneas. Depletion of KS was observed in the AC^{siChst5} group, while there were no obvious corneal structural changes in Str^{siChst5} mice. n>3. G, Alizarin red S staining of the corneal endothelium. The AC^{siChst5} group showed enlarged endothelial cells and diminished cellular boundaries (arrowhead). n=3. H, TEM of WT and *Chst5* knockdown mouse corneas. Quantification of corneal stromal collagen fibril diameter showed that the AC^{siChst5} group had significantly larger collagen fibrils than the other two groups. P<0.01, ANOVA.

central corneal thickness (CCT) decreased from 110.75 μm in AC^{siCon} to 88.88 μm in the AC^{siChst5} group (Figure 4F). AC^{siCon} had a similar CCT to that of WT mice.

Additionally, a lack of type IV collagens in the DM of MCD corneal sections was observed (Figure S6A in Supporting Information). Further evaluation using TEM indicated that the

https://doi.org/10.1007/s11427-023-2364-3

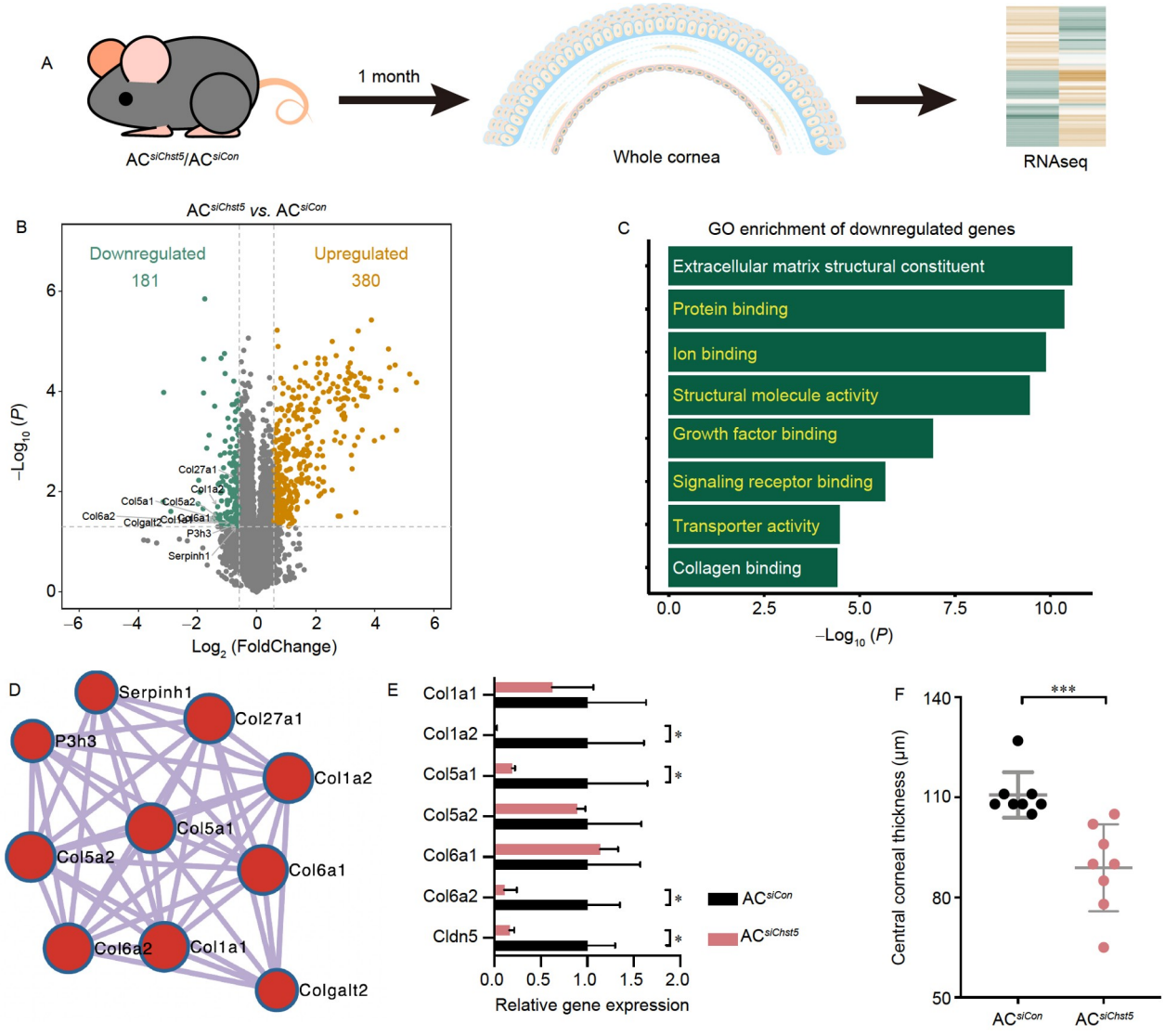

Figure 4. Transcriptomic analysis of endothelial *Chst5* knockdown mice. A, The whole cornea of $AC^{siChst5}$ and AC^{siCon} mice were collected at one month after intracameral injection and used for RNA sequencing. n=4. B, Volcano plot of DEGs between $AC^{siChst5}$ and AC^{siCon} groups. C, Top gene ontology terms of the downregulated genes in the $AC^{siChst5}$ group. D, Interactive network of the representative genes in the "extracellular matrix structural constituent" term. E, qPCR validation of the differentially downregulated collagen-related genes identified in the RNA sequencing. *Col1a2*, *Col5a1*, *Col6a2*, and *Cldn5* showed a significant decline in expression. n>3. Mann-Whitney U test. *, P<0.05. F, Central corneal thickness of $AC^{siChst5}$ and AC^{siCon} mice measured by OCT. n=8. Mann-Whitney U test. ***, P<0.001.

thickness of the MCD DM was significantly diminished in MCD corneas. This was accompanied by loosely arranged collagen fibrils and GAG deposits that had accumulated near the anterior surface of the DM (Figure S6B in Supporting Information). The alterations in collagen profiles induced by endothelial *Chst5* knockdown could be the primary cause of these abnormalities in the corneal DM.

CHST5 R50H mouse model recapitulates MCD phenotypes

The CHST6 protein consists of several crucial domains, including a sulfotransferase domain that spans amino acid residue 42 to 356 and two sulfate donor PAPS binding domains at amino acids 49–55 and 202–210 (Zhang et al., 2019). A homozygous CHST6 point mutation with the amino acid arginine at position 50 replaced by histidine (R50H) was found to cause bilateral MCD in a patient (Figure S7A in Supporting Information). OCT imaging revealed full-thickness corneal abnormalities in the patient (Figure S7A in Supporting Information). Both of the patient's parents were carriers of a heterozygous mutation at the same site (Figure S7B in Supporting Information). The R50 reside is situated in one of the two PAPS domains (Figure 5A) and is believed to disrupt sulfotransferase activity when mutated. To provide further evidence, we obtained the crystal structures of CHST6 with R50 and H50 interacting with the substrate PAP. The residue R50 has a similar structural basis and catalytic function as R78 of the tyrosylprotein sulfotransferase isoform 2 (TPST2) (Teramoto et al., 2013). When R50 is mutated to H50, the space between CHST6 and PAP increases due to the imidazole side chain, suggesting a decline in their interaction (Figure S7C in Supporting Information). A similar decrease in sulfotransferase activity was observed when TPST2 R78 was mutated to A78 (Teramoto et al., 2013).

The mouse CHST5 protein possesses a conserved amino acid

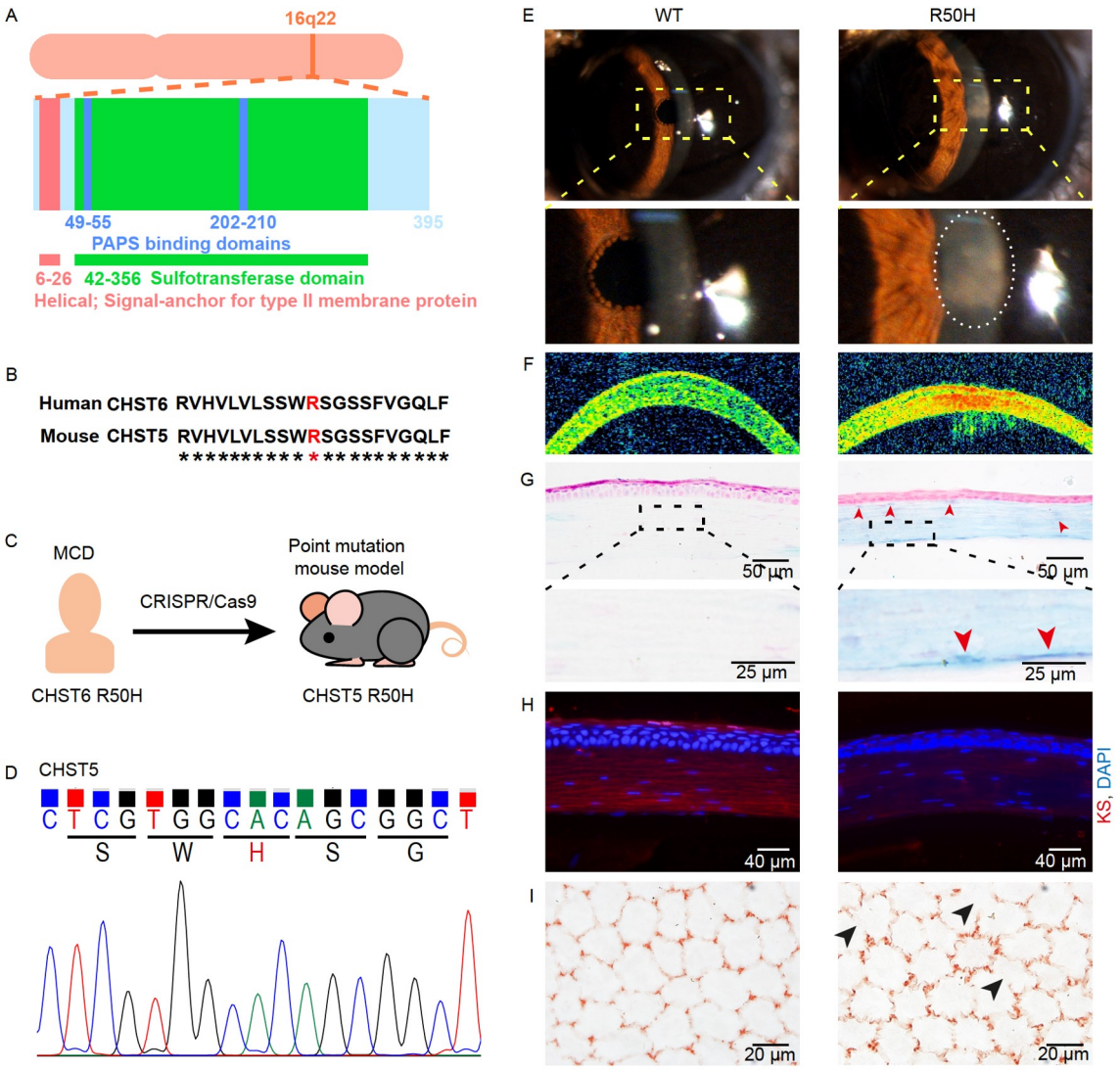

Figure 5. CHST5 R50H point mutation causes corneal endothelial lesions. A, Schematic diagram of the CHST6 protein structure. The protein contains two PAPS (3′-phospho-5′-adenylyl sulfate) domains locating at amino acid positions 49–55 and 202–210 (marked blue). The R50 amino acid is located in the first PAPS domain. B, Conservation analysis of the amino acid sequence around the mutation point. The amino acid arginine at position 50 is conserved between human CHST6 and mouse CHST5. C, A mouse model carrying CHST5 R50H amino acid mutation was created to mimic the CHST6 R50H MCD patient. D, Example of Sanger sequencing validation of the mouse model. All experimental littermates were homozygous at the mutation area. n=10. E and F, Slit lamp photos and OCT images of the WT and mutant mice. Corneal opacity (white dashed circle) and refractive index alteration (red areas in OCT) were observed in the CHST5 R50H mouse. n=10. G, Alcian blue staining of the CHST5 R50H mouse cornea. GAG deposits (red arrowhead) were present in the cornea. n=3. H, Lack of homogenous KS staining (white arrowhead) in the mutant cornea. I, Alizarin red S staining of the WT and CHST5 R50H mouse corneal endothelium. Diminished cellular boundaries (black arrowhead) were observed in the mutant endothelium. n=3.

R50 as the human CHST6 (Figure 5B). To mimic the MCD patient situation, a knock-in mouse model was generated with the CHST5 R50H mutation (*B6-Chst5*^{em1SEI}) (Figure 5C). Homozygous at the mutation site was confirmed in all mice used in this study (Figure 5D). Although the expression of the mutant CHST5 was not significantly decreased (Figure S8A and B in Supporting Information), loss of function in the protein was expected due to the observed bilateral corneal opacification (Figure 5E and F). Blue GAG deposits were observed in the corneal stroma of CHST5 R50H mice (Figure 5G), consistent with findings in human MCD corneas. Von Kossa staining ruled out the possibility of corneal calcification causing changes in acid mucopolysaccharide content in the same corneal sample (Figure S8C–E in Supporting Information). Sulfated KS staining indicated a lack of staining in the mutant cornea (Figure 5H). Endothelial cells in CHST5 R50H mice displayed diminished boundaries, altered shape, and elongated zig-zag lines (Figure 5I), which were absent in WT endothelial cells. The zig-zag line, which is ZO-1 positive in human endothelium, is indistinguishable under normal conditions, and its elongation suggests that the endothelium might be under stress. In conclusion, CHST5 R50H knock-in mice exhibited experimental MCD phenotypes and induced morphological changes in the corneal endothelium.

Intracameral *Chst5* overexpression rescues corneal impairments

To confirm the functional specificity of endothelial *Chst5*, we performed intracameral injection of WT *Chst5* in AC^{siChst5} and CHST5 R50H mice. Intracameral overexpression of WT *Chst5*

https://doi.org/10.1007/s11427-023-2364-3

(AC^{Chst5}) did not cause any changes in corneal transparency during the observation period (Figure S9A in Supporting Information). It increased endothelial *Chst5* expression by 57% when compared with the AC^{Con} endothelium (Figure S9B in Supporting Information). One year after knockdown of endothelial *Chst5*, all mice in the$AC^{siChst5}$ group displayed corneal reflectivity alterations (5/5) (Figure 6A). Supplementation with AC^{Chst5} one month after endothelial *Chst5* knockdown effectively restored corneal transparency for one year in 71.4% of mice (5/7) (Figure 6A).

When applied to 8-week-old CHST5 R50H mutant mice, AC^{Chst5} treatment slowed corneal opacity and maintained transparency in the pupil area in 33% of the tested mice (2/6), and reduced the number of GAG deposits, particularly in the endothelium (Figure 6B). The integrity of the endothelium was also preserved compared with the contralateral eye of the same mouse (Figure 6B). Although a decrease in the rate of endothelial lesions was observed in the rescued eye compared with the contralateral eye in homozygous CHST5 R50H mice, which lack functional *Chst5* from birth and have accumulated GAGs deposits

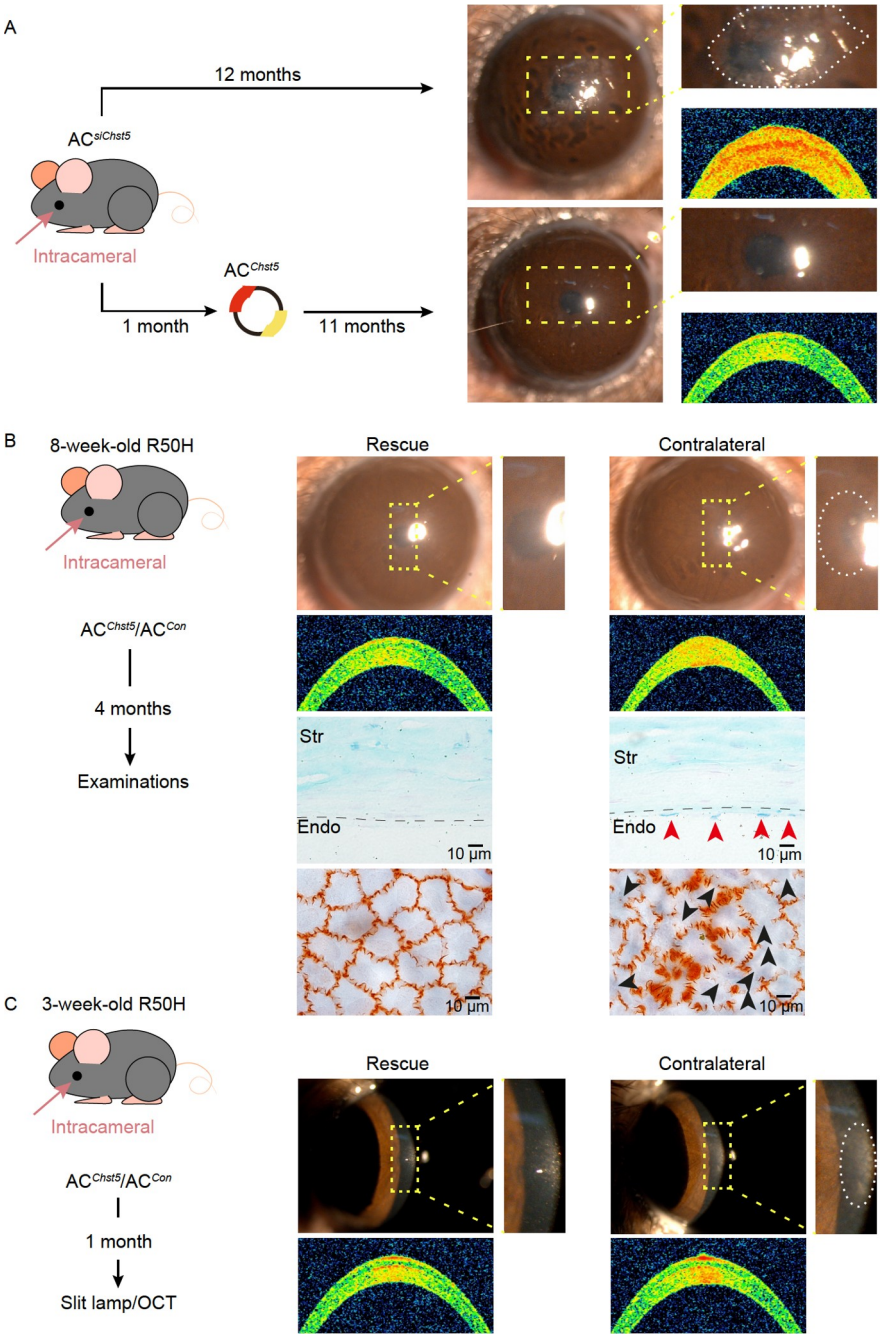

Figure 6. Addition of wild-type *Chst5* rescues corneal phenotypes. A, Rescue assay with $AC^{siChst5}$ mice. Corneal opacity and refractive index alteration were observed in all $AC^{siChst5}$ mice. n=5. After 11 months of intracameral overexpression of WT *Chst5*, 71% of the mice displayed better corneal phenotypes. n=7. B, Intracameral injection of WT *Chst5* into 8-week-old *Chst5* mutant mice. After about 4 months of rescue, 33% of the mice displayed retarded progression of corneal clouding around the pupil (white dashed circle) and reduced endothelial lesions. n=6. C, Intracameral injection of WT *Chst5* into 3-week-old *Chst5* mutant mice. After about 1 month of rescue, 40% of the mice displayed retarded progression of corneal opacification. n=5.

in the cornea, the improvement of corneal transparency under slit lamp was marginal (Figure 6B). To examine the efficacy of early treatment, we performed intracameral injection of WT *Chst5* in 3-week-old mutant mice and observed an improvement in corneal opacification in 40% of the mice (2/5) one month after treatment (Figure 6C). These observations suggest that intracameral injection of wild-type *Chst5* is a feasible approach to alleviate MCD, especially during the early stages of the disease.

The presented model (Figure 7) illustrates the normal and pathological states of the cornea. A healthy cornea produces CHST6 from the endothelium, leading to proper sulfation of GlcNAc at the 6-*O* position and synthesis of sulfated KS. Sulfated KS is crucial for organizing collagen fibril and maintaining cornea transparency. In contrast, the MCD cornea exhibits reduced functional CHST6 production due to loss-of-function mutations, leading to insufficiently sulphated KS. This results in a decrease in extracellular matrix constituents and the accumulation of GAG deposits in the intracellular and interfibrillar spaces, resulting in corneal opacity and thinning. As a result, surgical removal of the diseased endothelium is recommended to reduce the risk of MCD recurrence.

DISCUSSION

Macular corneal dystrophy is widely recognized as a stromal corneal dystrophy. In our study, we conducted a retrospective review of MCD recurrence over the past 30 years and found that PKP is more effective in decreasing the recurrent rate of MCD compared with DALK. Our investigation also revealed that the corneal endothelium has a higher concentration of sulfotransferase protein compared with the stroma and epithelium. Furthermore, we observed corneal endothelial deformation in mice carrying an endogenous homogenous CHST5 point mutation. Loss-of-function of wild-type *Chst5* in the corneal endothelium led to corneal opacification and accumulation of GAG deposits. Our study also demonstrated that intracameral injection of wild-type *Chst5* effectively blocked the progression of experimental MCD in both knockdown and mutant mice. In conclusion, our study provides evidence that MCD is associated with the corneal endothelium and offers clinical and experimental support for PKP treatment.

One more question is whether corneal endothelial transplantation alone could fully resolve MCD corneal opacity. Since MCD is often accompanied by deposits in the corneal stroma, it is possible that solely replacing the corneal endothelium may not improve visual acuity to a satisfactory extent. Moreover, MCD corneas consist of not fully sulfated KS and sometimes compensated chondroitin sulfate and dermatan sulfate (Plaas et al., 2001). It remains unknown whether exogenous sulfotransferase can properly sulfate the already existing diseased KS in the cornea and whether the re-sulfated KS and other compensated GAGs can be dissolved.

AAV-mediated gene therapy has been extensively studied in animal models with retinal disorders and has also been applied to treat inherited retinal degeneration caused by RPE65 deficiency (Bennett et al., 2016; Buch et al., 2008; Russell et al., 2017). Since MCD is an inherited eye disease caused by a single gene product deficiency and affects the outermost of the eye, it is a better candidate for gene therapy than retinal diseases. Although the corneal transparency of the 8-week-old mutant mice after rescue seems marginal, the treatment effect of overexpressing wild-type *Chst5* in younger mice (3-week-old) appears promising. Future investigations with embryos and young mice could be conducted to optimize the treatment effect.

Although a significant reduction of endothelial *Chst5* was detected in the $AC^{siChst5}$ group, the possibility that AAV9-siRNA entered the corneal stroma and knocked down the keratocyte *Chst5* cannot be excluded. To confirm that the MCD-like phenotypes observed in mice were predominantly induced by the lack of endothelial *Chst5*, we included an intrastromal injection control, and limited corneal impairments were observed. Creating an endothelium-conditional knockout

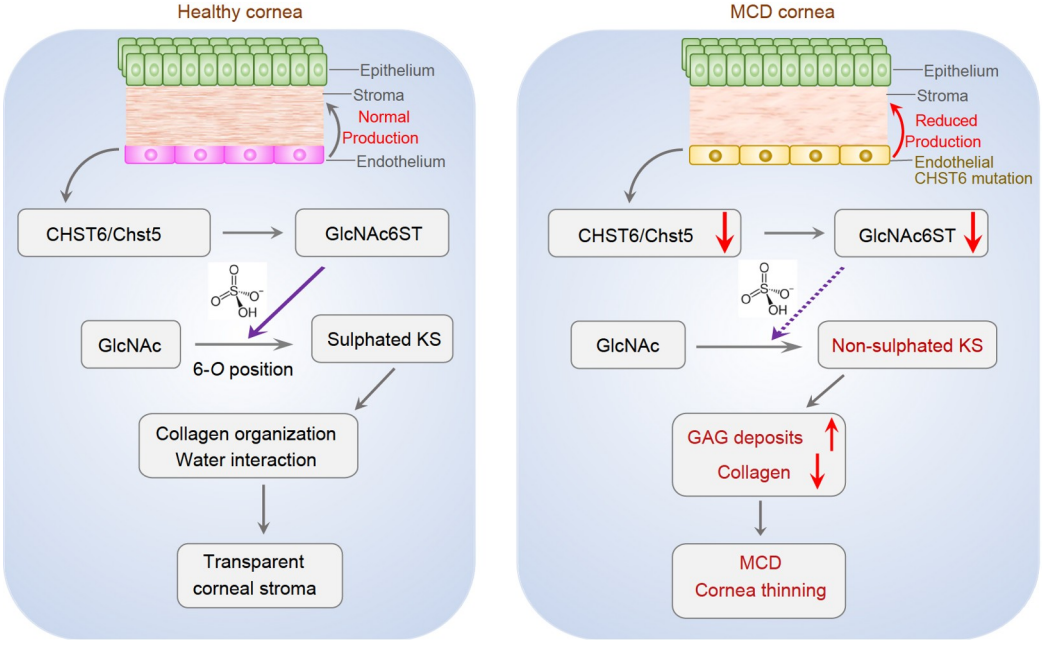

Figure 7. Schematic model of MCD pathogenesis.

https://doi.org/10.1007/s11427-023-2364-3

mouse using a corneal endothelium-Cre strain would be a more direct approach. However, there is a lack of robust mouse endothelial-specific genes to generate this Cre mouse. Both endothelial cells and keratocytes originate from the neural crest, and they share similar gene expression profiles in mice. We plan to identify potential endothelial-specific marker using mouse corneal single-cell sequencing datasets to make more robust mouse models.

Previous studies on *Chst5* knockout mice did not show visible corneal opacification but revealed a lack of properly sulfated KS in the cornea (Hayashida et al., 2006). The absence of corneal opacification in *Chst5*-null mice was attributed to the thin stroma (Hayashida et al., 2006). However, in lumican-deficient mice, which have a 40% reduction in stromal thickness compared with the wild-type mice, corneal haze and opacification were observed (Chakravarti et al., 1998; Chakravarti et al., 2000). Lumican, a member of the leucine-rich proteoglycan family, carries four KS side chains (Chakravarti et al., 1995; Puri et al., 2020). Loss of KS may significantly affect lumican function. In our study, we observed corneal transparency impairment in 11.3% of $AC^{siChst5}$ mice, and the deposit area lacks KS staining and was negative for calcification Von Kossa staining, suggesting that they more closely resemble MCD deposits rather than calcium deposits. The differences in our observations compared with those reported in previous *Chst5*-null mice studies (Hayashida et al., 2006) may be due to the different methods used to generate *Chst5*-deficient mice and the different examination methods applied.

All $AC^{siChst5}$ mice randomly selected in our study exhibited alcian blue positive deposits, even though not all of them displayed visible corneal opacification when examined under a slit lamp. This suggests that the deposition of materials could be an early event during the development of MCD. TEM revealed larger collagen fibrils in the posterior cornea of our mouse models, but did not observe vesicles filled with granular materials as reported in MCD patients (Jonasson et al., 1989) or extracellular materials between and among lamellae (Micali et al., 2014). As MCD is a progressive disease, most of our mouse models were still in the early stage of the disease. Amyloid deposits were observed in the corneal stroma of CHST5 R50H mice at 15 weeks of age. We will continue to collect corneas from *Chst5*-deficient mice at different time points and analyze their GAG profiles by liquid chromatography/mass spectrometry to further investigate the disease progression. Additionally, corneal reflectivity changes will be monitored over time with OCT.

Although clinical and experimental data suggest that the endothelial layer plays a crucial role in MCD, it remains unclear how endothelial CHST6 can penetrate the thick DM and regulate the stromal KS sulphation. Stromal sulphated KS is highly negatively charged and hydrophilic (Quantock et al., 2010), which can cause stromal swelling. The endothelium is responsible to dehydrate the stroma and to transport nutrients from the aqueous humor to the stroma (Bonanno, 2012). The core structure of corneal KS is synthesized in the rough endoplasmic reticulum and Golgi apparatus and is then processed by various enzymes, including cGn6ST (Quantock et al., 2010). If endothelial cGn6ST can translocate to the stroma, further investigation is needed to determine how the enzyme processes its substrate.

In recent years, significant progress has been made in understanding of the onset and treatment of ocular diseases (Liu et al., 2022; Xue et al., 2022). Fifty years ago, it was reported that abnormal deposits of acid mucopolysaccharide were found in the corneal endothelium and DM of MCD corneal samples, indicating that the endothelium might play a primary role in the pathogenesis of MCD (Snip et al., 1973). Similarly, clinical observations suggested that MCD exhibits more abnormalities in the posterior cornea (Klintworth, 2009; Palka et al., 2010; Rubinstein et al., 2016). However, experimental evidence supporting the role of corneal endothelium in MCD progression was lacking until our mouse models revealed its pivotal role in the disease. Our findings suggest that corneal endothelial cells are involved in the pathogenesis and recurrence of MCD, and PKP can be a suitable surgical option for treating advanced MCD.

MATERIALS AND METHODS

Paraffin sectioning and immunohistochemistry

Corneas from MCD patients and mice were fixed in 4% paraformaldehyde at 4°C, embedded in paraffin, and sectioned into 4 μm thick slices. Deparaffinization of the sections was performed by placing the slides to xylene three times for 10 min each, followed by sequential immersion in 100%, 95%, 90%, 85% ethanol for 2 min each, and finally rinsed with cold tap water. Antigen retrieval was achieved by boiling the sections in 1× Citrate Antigen Retrieval Solution (Maxim Biotechnologies, Fuzhou, China) for 5 min, followed by washing with tap water. The slides were then treated with 3% H_2O_2 for 5 min and washed with PBS three times. Next, the slides were blocked in 10% bovine serum albumin (BSA) (Solarbio, Beijing, China) for 1 h. Primary antibodies, Anti-CHST6 (1:200, Abcam, UK) diluted in NCM Universal Antibody Diluent (New Cell & Molecular, Suzhou, China), and anti-CHST5 (1:200, Everest Biotech, UK) diluted in 10% BSA, were applied. After incubating the primary antibody at 4°C overnight, slides were washed with PBS and incubated with secondary antibody (MaxVision TM HRP-Polymer anti-Mouse/Rabbit IHC Kit, Maxim Biotechnologies) for 1.5 h, then washed with PBS for three times. The staining was developed with DAB solution (1:20, ZSGB-Bio, Beijing, China) for 1.5 min followed by counterstaining with Hematoxylin for 80 s. The slides were then mounted and observed.

Exome sequencing for *CHST6* mutation detection

To detect *CHST6* mutation, 2 mL peripheral blood was collected from the MCD pedigree with consent forms obtained. Genomic DNA was extracted from the peripheral blood (QIAamp, Qiagen, Germany) and subjected to exome sequencing on Illumina HiSeq X Ten System. The sequencing and subsequent data analysis were carried out by MyGenostics Inc. (Beijing, China).

Construction of CHST5 R50H point mutation mouse

CRISPR/Cas9 system was utilized to induce the R50H point mutation in the *Chst5* gene through a knock-in strategy. sgRNAs were designed to target the *Chst5* exon 2. The *in vitro* sgRNA activity was tested, and the most efficient sgRNA, *Chst5*-g1 ACTGTCCTCGTGGCGCTCGGG, with a cutting efficacy of 94%, was selected. The mouse model was generated and bred by Beijing Viewsolid Biotech Co. Ltd. To confirm the point mutation, specific primers were designed to amplify the region containing the mutation point, and the gel electrophoresis products were

collected for Sanger sequencing. The mice carrying homozygous point mutation were used for further experiments. The standardized nomenclature of our mouse strain is *B6-Chst5*^{em1SEI}. Validation primers: M-PM-T6-FP: 5′-GTCATACAACACGGAAGCACAC-3′; M-PM-T6-RP: 5′-GCATAGGAACACTGAGCGGATC-3′.

Alcian blue staining

A 1% alcian blue solution was prepared by dissolving Alcian Blue 8GX powder (Sigma-Aldrich, USA) in 3% acetic acid. Cryosection slides of 7 μm thickness were fixed with neutral buffered formalin solution for 5 min, followed by rinsing in 3% acetic acid for 3 min. The slides were then stained with 1% alcian blue solution for 30 min, washed with 3% acetic acid, and counterstained with Nuclear Fast Red (Beyotime, Shanghai, China) for 5 min. After dehydration in 95% ethanol, the slides were mounted.

Von Kossa staining

The cryosection slides were heated at 60°C for 15 min. The slides were covered with Von Kossa solution (Wuhan Servicebio, Wuhan, China) for 40 min under ultraviolet light. After rinsing with distilled water, the slides were stained with hematoxylin and eosin.

Alizarin red S staining

The isolated mouse cornea was placed with the endothelium facing up and rinsed with trypan blue for 1 min. After washing with PBS three times, the cornea was covered with alizarin red S solution (Wuhan Servicebio) for 90 s. The cornea was then washed with PBS and flattened by making four radical cuts from the peripheral. Next, the cornea was placed onto a slide with the endothelial layer facing up and imaged under a microscope.

AAV9 plasmids design and packaging

The AAV9 plasmids were packaged by Shanghai GeneChemCo., Ltd. To generate the *Chst5* knockdown plasmid, shRNA oligos targeting three positions of the mouse *Chst5* (NM_019950) were designed and inserted into the GV478 vector (U6-MCS-CAG-EGFP) using the *BsmBI* restriction site. The knockdown control sequence was designed as 5′-CGCTGAGTACTTCGAAATGTC-3′. To test the knockdown efficiency, the plasmids were transfected into HEK 293T cells, and proteins were collected. The gene knockdown efficacy was examined using Western blot against the FLAG tag with anti-FLAG M2 antibody (1:2,000, Sigma-Aldrich) and goat anti-mouse IgG-HRP antibody (1:4,000, Santa Cruz, USA). A pair of oligos (ACGCTGCCCT- TTGCCAAGATT; AATCTTGGCAAAGGGCAGCGT) with the highest *Chst5* knockdown efficiency was selected for virus packaging. For the overexpression AAV9 plasmid of the wild-type *Chst5*, the full-length *Chst5* gene was amplified with primer pairs and inserted into the GV461 vector (CMV-betaGlobin-MCS-SV40 PolyA) using the *BamHI* and *HindIII* restriction sites. *Chst5* amplification primers: F: 5′-GAGGTAGTGGAATGGATCCCGCCACCATGCGGCTACCCCGTTTCTC-3′; R: 5′- GCCTCAGCTATTTAAAGCTAAGATTCCGGTTGCTTCTCCG-3′. For the Kera knockdown plasmid, shRNA oligos targeting three positions of the mouse *Kera* (NM_008438) gene were designed and inserted into the GV478 vector (U6-MCS-CAG-EGFP) using the *BsmBI* restriction site. The knockdown control sequence was designed as 5′-CGCTGAGTACTTCGAA- ATGTC-3′. The pair of oligos (GCTAGAAACAAAGT- ATCCAGA; TCTGGATACTTTGTTTCTAGC) with the highest *Kera* knockdown efficiency was selected for virus packaging.

In vivo injection of AAV9 plasmids

Eight-week-old C57BL/6J mice were randomly assigned to receive AAV-shRNA injection. For all injection experiments, 1 μL virus (10^{12} v.g. mL^{-1}) was injected into one eye of the mouse using a 36-gauge NanoFil syringe (World Precision Instruments Inc, USA). For intrastromal injection, the needle was inserted obliquely with the bevel down into the paracentral corneal stroma under a surgical microscope. When the needle reached the center of the cornea, 1 μL of the solution was injected. For intracameral injection, the needle was inserted obliquely with the bevel down from the limbus, and went through the stroma, penetrating the anterior chamber when the needle reached the center of the cornea. After removing the needle, the puncture point was pressed with a cotton swab for 30 s to prevent aqueous humor leakage. For the rescue assay, AAV plasmids were injected into the eye again one month after the first injection. Mouse corneas were examined using anterior segment OCT (Optovue RTVue XR, USA), and greyscale or false-color images were generated to indicate corneal optical properties and refractive indices. For gene expression examination, corneas were collected two weeks after injection. For histological examination, corneas were collected at least two months post-injection.

Dissection and digestion of corneas

Mice were euthanized and enucleated eyeballs were placed in a dish filled with PBS. A 1 mL syringe needle was used to create a scissor incision by a circular cut with Vannas scissors (Suzhou Mingren, Suzhou, China), and the iris was gently scraped off under a stereoscope. The corneal endothelial layer was gently peeled with surgical forceps (Suzhou Mingren). The remaining corneal tissue, including the epithelial and stromal layers, was transferred to a 96-well plate and digested with 100 μL of 15 mg mL^{-1} Dispase II (Roche, Switzerland) at 37°C for 15 min. The epithelium was scraped off from the stroma with forceps. The dissected epithelium, stroma, and endothelium were transferred into 2 mL tubes and rapidly frozen by immersing in liquid nitrogen. The samples were kept at −80°C until further use. The dissection procedure for human corneal samples was similar to that of the mouse cornea, except that after the corneal endothelium was removed, the remaining tissue was transferred to a 24-well plate and digested with 1 mL 2.4 U mL^{-1} Dispase II at 37°C for 30 min.

RNA extraction, cDNA synthesis and qPCR analysis

Total RNA was extracted from the samples using the TransZol Up Plus RNA Kit (TransGen Biotech, Beijing, China) according to the manufacturer's instructions. The concentration and purity of the RNA were measured using a NanoDrop One spectrophotometer (Thermo Fisher Scientific, USA). Complementary DNA (cDNA) was synthesized from the extracted RNA using the PrimeScript

cDNA Synthesis Kit (TaKaRa Bio, Dalian, China) following the manufacturer's protocol, and stored at −20°C until further use. The qPCR reaction was performed using Premix Taq (TaKaRa, Beijing, China), and the qPCR primers used are listed in Table S1 in Supporting Information.

RNA sequencing of mouse cornea

The entire corneas from $AC^{siChst5}$ and AC^{siCon} mice were harvested for RNA sequencing. The RNA sequencing was carried out by Aksomics Inc. (Shanghai, China). The cDNA library was constructed with KAPA Stranded RNA-Seq Library Prep Kit (Illumina, USA). The completed libraries were qualified using the Agilent 2100 Bioanalyzer, quantified using the absolute quantification qPCR method, and sequenced on the Illumina HiSeq 4000 instrument. DEGs were identified as having a fold-change ($AC^{siChst5}$ *vs.* AC^{siCon}) exceeding 1.5 and *P*-values less than 0.05.

Microarray gene expression analysis of human corneal endothelial cells

The corneal endothelium from three MCD patients and two healthy donors was collected and stored in 50 μL Trizol at −80°C for subsequent analysis. Microarray analysis was conducted by Aksomics Inc. The samples were labeled with the Agilent Quick Amp Labeling Kit and hybridized with Agilent SureHyb Hybridization Chambers. The microarray slides were scanned with the Agilent DNA Microarray Scanner, and the data was collected using the Agilent Feature Extraction software (v11.0.0.1). Data normalization was performed using Agilent GeneSpring GX v12.1. DEGs were defined as having a fold-change (MCD *vs.* Healthy) exceeding 2.0 and *P*-values less than 0.05.

Immunofluorescence staining

The mouse eye was embedded in the Tissue-Tek O.C.T. compound (Sakura Finetek, Japan) and sectioned into 7 μm thick sections. The sections were subjected to immunofluorescence staining with primary antibodies against KS (1:10, 4B3/D10, Santa Cruz; 5D4, MD Bioproducts, USA), Krt12 (1:200, Abcam), followed by incubation with a fluorescein-conjugated secondary antibody (Goat Anti-Mouse IgG H&L, Alexa Fluor 594, 1:50, Abcam). The sections were counterstained with DAPI and observed under a confocal microscope (Zeiss, Germany) or Revolve Fluorescence Microscope (Echo, USA).

Transmission electron microscopy

The samples were trimmed to less than 1 mm^3 and fixed with 2.5% glutaraldehyde in 100 mmol L^{-1} Sorensen's phosphate buffer (pH 7.0) at 4°C for at least 4 h. Subsequently, samples were washed with 0.1 mol L^{-1} Sorenson's phosphate buffer (pH 7.2) and then subjected to a secondary fixation with 1% osmium tetroxide. The samples were dehydrated sequentially in 70%, 80%, 95% and 100% acetone and cleared in propylene oxide. They were then infiltrated in a series of mixtures of Epoxy 812 embedding medium (Sigma-Aldrich) and propylene oxide, in ratios of 2:1 for 0.5 h at room temperature, 1:2 for 1.5 h at 37°C, and pure embedding medium for 3 h at 37°C. After embedding in a mould, the samples were polymerized at 37°C for 24 h, 45°C for 24 h, and 60°C for 24 h. Ultrathin sections of 70 nm were made using an ultramicrotome (Reichert-Jung, USA) and placed on a 200-mesh grid. The ultrathin sections were stained with saturated uranyl acetate and lead citrate for 15 min each. The stained sections were examined under a transmission electron microscope (JEOL, USA).

Data availability

Original data created for the study will be available upon publication. Mouse transcriptome data have been deposited in the Genome Sequence Archive (GSA, https://ngdc.cncb.ac.cn/gsa/) with the accession number CRA005419. The human microarray data has been deposited in the OMIX Database (https://ngdc.cncb.ac.cn/omix/) under the accession number OMIX730.

Compliance and ethics

The authors declare no competing interest. This study was conducted in compliance with the tenets of the Declaration of Helsinki and was approved by the Ethics Committee of Qingdao Eye Hospital (2021-09). Informed consent was obtained from the participants involved in the study. The use of data in this was approved by the Academic Board of Qingdao Eye Institute. Corneal tissues from healthy donors were obtained from the Eye Bank of Qingdao Eye Hospital, while diseased corneas from MCD patients were collected during corneal transplantation surgeries. The animal study protocols were approved by the Animal Investigation Committee of the Eye Institute of Shandong First Medical University. All animal procedures were performed in accordance with The Association for Research in Vision and Ophthalmology (ARVO) statement.

Acknowledgement

This work was supported by the Shandong Provincial Natural Science Foundation (ZR2020QH140), the National Natural Science Foundation of China (82101091), the Academic Promotion Program of Shandong First Medical University (2019ZL001, 2019RC008), the Shandong Provincial Key Research and Development Program (2021ZDSYS14). The authors would like to thank Dr. Can Zhao for refining the microinjection method, Ting Liu for providing corneal paraffin sections from MCD patients, Rui Cao and Li Gao for providing human corneal tissues, Xia Qi and Guoying Liu for refining alcian blue staining protocol.

Supporting information

The supporting information is available online at https://doi.org/10.1007/s11427-023-2364-3. The supporting materials are published as submitted, without typesetting or editing. The responsibility for scientific accuracy and content remains entirely with the authors.

References

Akama, T.O., Nakayama, J., Nishida, K., Hiraoka, N., Suzuki, M., McAuliffe, J., Hindsgaul, O., Fukuda, M., and Fukuda, M.N. (2001). Human corneal GlcNAc 6-*O*-sulfotransferase and mouse intestinal GlcNAc 6-*O*-sulfotransferase both produce keratan sulfate. J Biol Chem 276, 16271–16278.

Akama, T.O., Nishida, K., Nakayama, J., Watanabe, H., Ozaki, K., Nakamura, T., Dota, A., Kawasaki, S., Inoue, Y., Maeda, N., et al. (2000). Macular corneal dystrophy type I and type II are caused by distinct mutations in a new sulphotransferase gene. Nat Genet 26, 237–241.

Bennett, J., Wellman, J., Marshall, K.A., McCague, S., Ashtari, M., DiStefano-Pappas, J., Elci, O.U., Chung, D.C., Sun, J., Wright, J.F., et al. (2016). Safety and durability of effect of contralateral-eye administration of AAV2 gene therapy in patients with childhood-onset blindness caused by RPE65 mutations: a follow-on phase 1 trial. Lancet 388, 661–672.

Bonanno, J.A. (2012). Molecular mechanisms underlying the corneal endothelial pump. Exp Eye Res 95, 2–7.

Buch, P.K., Bainbridge, J.W., and Ali, R.R. (2008). AAV-mediated gene therapy for retinal disorders: from mouse to man. Gene Ther 15, 849–857.

Caterson, B., and Melrose, J. (2018). Keratan sulfate, a complex glycosaminoglycan with unique functional capability. Glycobiology 28, 182–206.

Chakravarti, S., Magnuson, T., Lass, J.H., Jepsen, K.J., LaMantia, C., and Carroll, H. (1998). Lumican regulates collagen fibril assembly: skin fragility and corneal opacity in the absence of lumican. J Cell Biol 141, 1277–1286.

Chakravarti, S., Petroll, W.M., Hassell, J.R., Jester, J.V., Lass, J.H., Paul, J., and Birk, D. E. (2000). Corneal opacity in lumican-null mice: defects in collagen fibril structure and packing in the posterior stroma. Invest Ophthalmol Vis Sci 41, 3365–3373.

Chakravarti, S., Stallings, R.L., SundarRaj, N., Cornuet, P.K., and Hassell, J.R. (1995).

Primary structure of human lumican (keratan sulfate proteoglycan) and localization of the gene (LUM) to chromosome 12q21.3-q22. Genomics 27, 481–488.
Cheng, J., Qi, X., Zhao, J., Zhai, H., and Xie, L. (2013). Comparison of penetrating keratoplasty and deep lamellar keratoplasty for macular corneal dystrophy and risk factors of recurrence. Ophthalmology 120, 34–39.
Gain, P., Jullienne, R., He, Z., Aldossary, M., Acquart, S., Cognasse, F., and Thuret, G. (2016). Global survey of corneal transplantation and eye banking. JAMA Ophthalmol 134, 167–173.
Hassell, J.R., Newsome, D.A., Krachmer, J.H., and Rodrigues, M.M. (1980). Macular corneal dystrophy: failure to synthesize a mature keratan sulfate proteoglycan. Proc Natl Acad Sci USA 77, 3705–3709.
Hayashida, Y., Akama, T.O., Beecher, N., Lewis, P., Young, R.D., Meek, K.M., Kerr, B., Hughes, C.E., Caterson, B., Tanigami, A., et al. (2006). Matrix morphogenesis in cornea is mediated by the modification of keratan sulfate by GlcNAc 6-*O*-sulfotransferase. Proc Natl Acad Sci USA 103, 13333–13338.
Jonasson, F., Johannsson, J.H., Garner, A., and Rice, N.S.C. (1989). Macular corneal dystrophy in Iceland. Eye 3, 446–454.
Kawashima, M., Kawakita, T., Den, S., Shimmura, S., Tsubota, K., and Shimazaki, J. (2006). Comparison of deep lamellar keratoplasty and penetrating keratoplasty for lattice and macular corneal dystrophies. Am J Ophthalmol 142, 304–309.
Klintworth, G.K. (2009). Corneal dystrophies. Orphanet J Rare Dis 4, 7.
Klintworth, G.K., Reed, J., Stainer, G.A., and Binder, P.S. (1983). Recurrence of macular corneal dystrophy within grafts. Am J Ophthalmology 95, 60–72.
Lisch, W., and Weiss, J.S. (2019). Clinical and genetic update of corneal dystrophies. Exp Eye Res 186, 107715.
Liu, X., Khodeiry, M.M., Lin, D., Sun, Y., Zhang, Q., Wang, J., Lee, R.K., and Wang, N. (2022). The association of cerebrospinal fluid pressure with optic nerve head and macular vessel density. Sci China Life Sci 65, 1171–1180.
Micali, A., Pisani, A., Puzzolo, D., Nowińska, A., Wylegala, E., Teper, S., Czajka, E., Roszkowska, A.M., Orzechowska-Wylegala, B., and Aragona, P. (2014). Macular corneal dystrophy. Ophthalmology 121, 1164–1173.
Palka, B.P., Sotozono, C., Tanioka, H., Akama, T.O., Yagi, N., Boote, C., Young, R.D., Meek, K.M., Kinoshita, S., and Quantock, A.J. (2010). Structural collagen alterations in macular corneal dystrophy occur mainly in the posterior stroma. Curr Eye Res 35, 580–586.
Plaas, A.H., West, L.A., Thonar, E.J.A., Karcioglu, Z.A., Smith, C.J., Klintworth, G.K., and Hascall, V.C. (2001). Altered fine structures of corneal and skeletal keratan sulfate and chondroitin/dermatan sulfate in macular corneal dystrophy. J Biol Chem 276, 39788–39796.
Puri, S., Coulson-Thomas, Y.M., Gesteira, T.F., and Coulson-Thomas, V.J. (2020). Distribution and function of glycosaminoglycans and proteoglycans in the development, homeostasis and pathology of the ocular surface. Front Cell Dev Biol 8, 731.
Quantock, A.J., Young, R.D., and Akama, T.O. (2010). Structural and biochemical aspects of keratan sulphate in the cornea. Cell Mol Life Sci 67, 891–906.
Reddy, J.C., Murthy, S.I., Vaddavalli, P.K., Garg, P., Ramappa, M., Chaurasia, S., Rathi, V., and Sangwan, V.S. (2015). Clinical outcomes and risk factors for graft failure after deep anterior lamellar keratoplasty and penetrating keratoplasty for macular corneal dystrophy. Cornea 34, 171–176.
Rubinstein, Y., Weiner, C., Einan-Lifshitz, A., Chetrit, N., Shoshany, N., Zadok, D., Avni, I., and Pras, E. (2016). Macular corneal dystrophy and posterior corneal abnormalities. Cornea 35, 1605–1610.
Russell, S., Bennett, J., Wellman, J.A., Chung, D.C., Yu, Z.F., Tillman, A., Wittes, J., Pappas, J., Elci, O., McCague, S., et al. (2017). Efficacy and safety of voretigene neparvovec (AAV2-hRPE65v2) in patients with RPE65-mediated inherited retinal dystrophy: a randomised, controlled, open-label, phase 3 trial. Lancet 390, 849–860.
Snip, R.C., Kenyon, K.R., and Green, W.R. (1973). Macular corneal dystrophy: ultrastructural pathology of corneal endothelium and Descemet's membrane. Invest Ophthalmol 12, 88–97.
Teramoto, T., Fujikawa, Y., Kawaguchi, Y., Kurogi, K., Soejima, M., Adachi, R., Nakanishi, Y., Mishiro-Sato, E., Liu, M.C., Sakakibara, Y., et al. (2013). Crystal structure of human tyrosylprotein sulfotransferase-2 reveals the mechanism of protein tyrosine sulfation reaction. Nat Commun 4, 1572.
Weiss, J.S., Møller, H.U., Aldave, A.J., Seitz, B., Bredrup, C., Kivelä, T., Munier, F.L., Rapuano, C.J., Nischal, K.K., Kim, E.K., et al. (2015). IC3D classification of corneal dystrophies—edition 2. Cornea 34, 117–159.
Xue, B., Wang, P., Yu, W., Feng, J., Li, J., Zhao, R., Yang, Z., Yan, X., and Duan, H. (2022). CD146 as a promising therapeutic target for retinal and choroidal neovascularization diseases. Sci China Life Sci 65, 1157–1170.
Young, R.D., Tudor, D., Hayes, A.J., Kerr, B., Hayashida, Y., Nishida, K., Meek, K.M., Caterson, B., and Quantock, A.J. (2005). Atypical composition and ultrastructure of proteoglycans in the mouse corneal stroma. Invest Ophthalmol Vis Sci 46, 1973–1978.
Zhang, J., Wu, D., Li, Y., Fan, Y., Dai, Y., and Xu, J. (2019). A comprehensive evaluation of 181 reported CHST6 variants in patients with macular corneal dystrophy. Aging 11, 1019–1029.